http://www.jstage.jst.go.jp/browse/biophysics

BIOPHYSICS

REVIEW

Vol. 9, pp. 31–36 (2013)
doi: 10.2142/biophysics.9.31

# Mechanism of the nucleotidyl-transfer reaction in DNA polymerase revealed by time-resolved protein crystallography

Teruya Nakamura[1,2], Ye Zhao[2,3], Yuriko Yamagata[1], Yue-jin Hua[3] and Wei Yang[2]

[1]*Graduate School of Pharmaceutical Sciences, Kumamoto University, Kumamoto 862-0973, Japan*
[2]*Laboratory of Molecular Biology, National Institute of Diabetes and Digestive and Kidney Diseases, National Institutes of Health, Bethesda, Maryland 20892, USA*
[3]*Institute of Nuclear-Agricultural Sciences, Zhejiang University, Hangzhou 310029, China*

Received February 14, 2013; accepted March 24, 2013

**Nucleotidyl-transfer reaction catalyzed by DNA polymerase is a fundamental enzymatic reaction for DNA synthesis. Until now, a number of structural and kinetic studies on DNA polymerases have proposed a two-metal-ion mechanism of the nucleotidyl-transfer reaction. However, the actual reaction process has never been visualized. Recently, we have followed the nucleotidyl-transfer reaction process by human DNA polymerase η using time-resolved protein crystallography. In sequence, two $Mg^{2+}$ ions bind to the active site, the nucleophile 3′-OH is deprotonated, the deoxyribose at the primer end converts from C2′-endo to C3′-endo, and the nucleophile and the α-phosphate of the substrate dATP approach each other to form the new bond. In this process, we observed transient elements, which are a water molecule to deprotonate the 3′-OH and an additional $Mg^{2+}$ ion to stabilize the intermediate state. Particularly, the third $Mg^{2+}$ ion observed in this study may be a general feature of the two-metal-ion mechanism.**

**Key words:** DNA polymerase, nucleotidyl-transfer reaction, $Mg^{2+}$ ion, time-resolved protein crystallography

DNA polymerases are widely distributed in living organisms and play an important role in DNA synthesis. Until now, a number of DNA polymerases have been discovered and grouped into six different families (A, B, C, D, X and Y) based on amino acid sequence homologies and structural studies[1,2]. These families operate at different stages in DNA replication. Previous kinetic, mutational and structural studies have proposed that DNA polymerases share a two-metal-ion mechanism for the nucleotidyl-transfer reaction[3–6]. Recently, we have followed the reaction process of human DNA polymerase η in the Y-family by time-resolved protein crystallography, and observed structural changes and transient elements associated with the reaction[7]. In this review, we will describe the background of the reaction mechanism of DNA polymerase and introduce the results obtained from our recent research.

## DNA polymerase and the reaction mechanism

DNA polymerase incorporates a dNTP complementary to the templating base and catalyzes the formation of a phosphodiester bond between the 3′-OH of the primer strand and the α phosphorus of the dNTP. In order to understand the nucleotidyl-transfer reaction, crystal structures of a number of DNA polymerases from several families have been determined. As examples, structures of the A-, B-, X- and Y-family DNA polymerases, which are well-studied, are shown in Figures 1 and 2[8–10]. In general, the A- and B-family DNA polymerases are involved in DNA replication during the cell cycle, and the X-family DNA polymerases have a key role in DNA repair. The A- and B-family DNA polymerases

Corresponding author: Teruya Nakamura, Graduate School of Pharmaceutical Sciences, Kumamoto University, 5-1 Oe-honmachi, Chuo-ku, Kumamoto 862-0973, Japan.
e-mail: tnaka@gpo.kumamoto-u.ac.jp

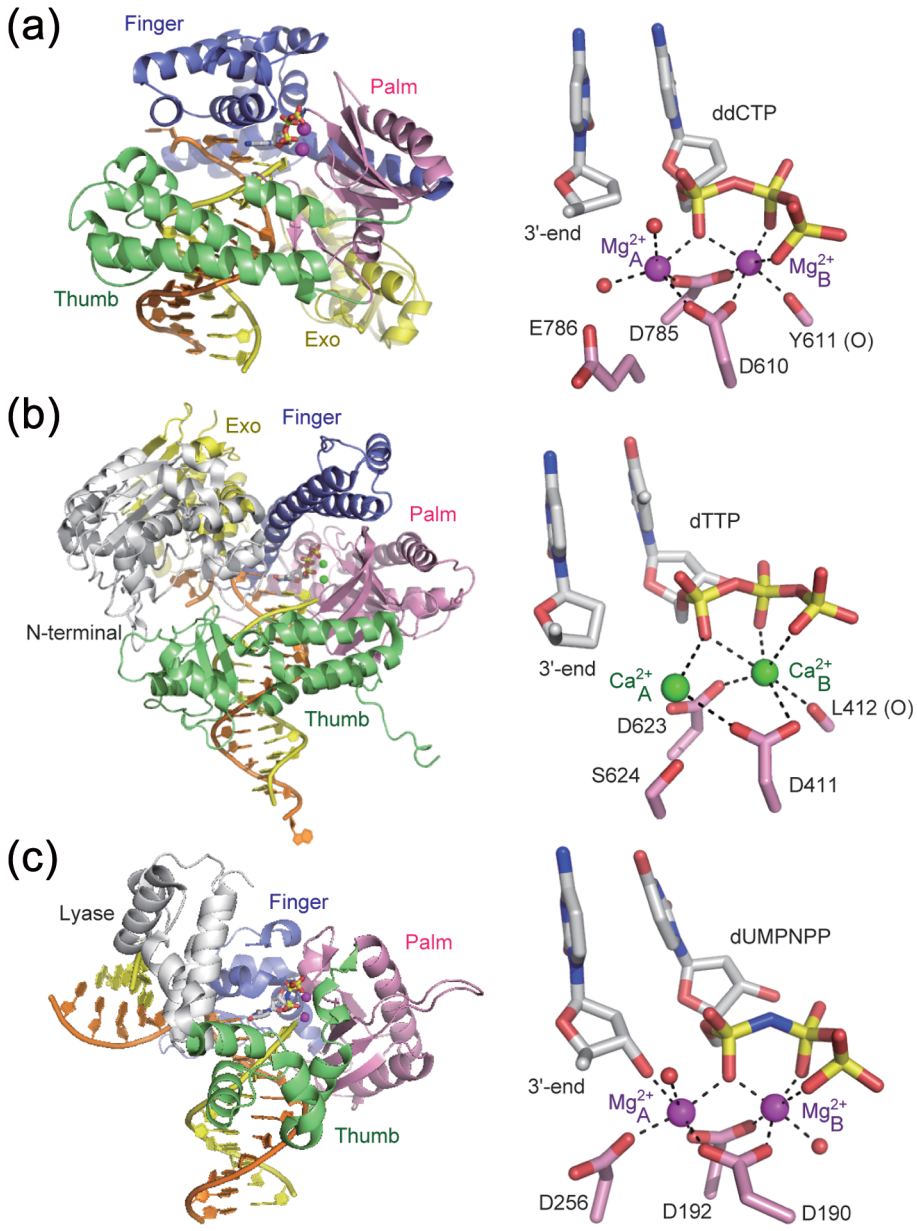


**Figure 1** Structures of DNA polymerases (left, overall structures; right, active site structures). The palm, finger and thumb domains are shown in different colors. Exo, exonuclease domain; N-terminal, N-terminal domain; Lyase, lyase domain. The template and primer strands are colored in orange and yellow, respectively. Primer end, an incoming nucleotide and active site residues are shown as sticks. Water molecules are shown as red spheres. Dashed lines indicate $Mg^{2+}$ or $Ca^{2+}$ coordination. (a) *Taq* DNA polymerase (A-family, PDB code 3KTQ)[8]. (b) RB69 DNA polymerase α (B-family, PDB code 1IG9)[9]. (c) Human DNA polymerase β (X-family, PDB code 2FMS)[10].

have a right-hand like overall architecture with the palm, finger and thumb domains, which hold a double-stranded DNA (Fig. 1a, b). In the X-family DNA polymerases, the palm domain is not homologous with those of the A- and B-families, but the overall architecture still resembles a right hand (Fig. 1c, Domain annotation for the finger and thumb domains is defined according to that of canonical DNA polymerases.).

The Y-family DNA polymerases including DNA polymerase η are specialized in translesion DNA synthesis. Although the Y-family DNA polymerases share little sequence homology with the A-, B- and X-family DNA polymerases, they also have a right-hand like overall architecture with the palm, finger, thumb domains and an additional C-terminal domain[11]. The C-terminal domain is called little finger domain in accordance with an analogy to a right hand because of its role in holding a DNA at the opposite side of the thumb domain (Fig. 2a, discussed later).

In spite of the structural diversity, all DNA polymerases crystallized so far have a similar active site structure. A

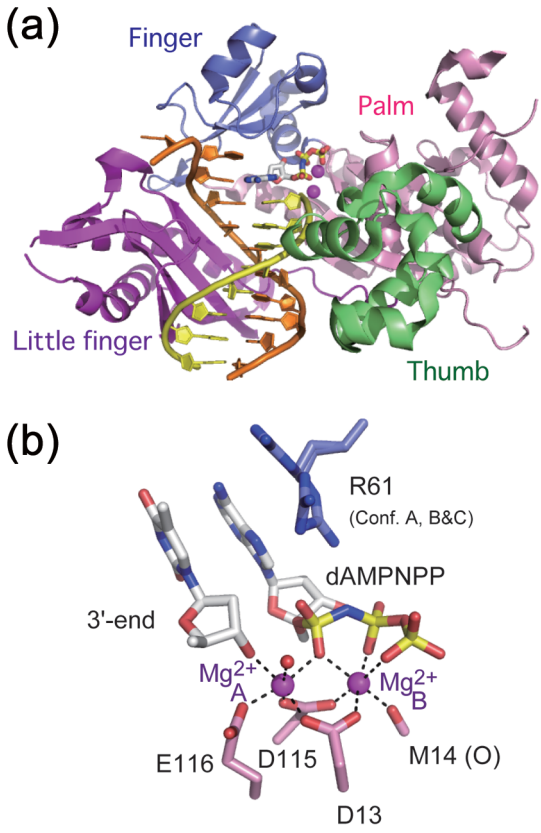


**Figure 2** Structure of Pol η. (a) Overall structure of the ternary complex of Pol η with normal DNA and dAMPNPP (PDB code 3MR2)[15]. The palm, finger, thumb and little finger domains are shown in different colors. (b) Active site of Pol η.

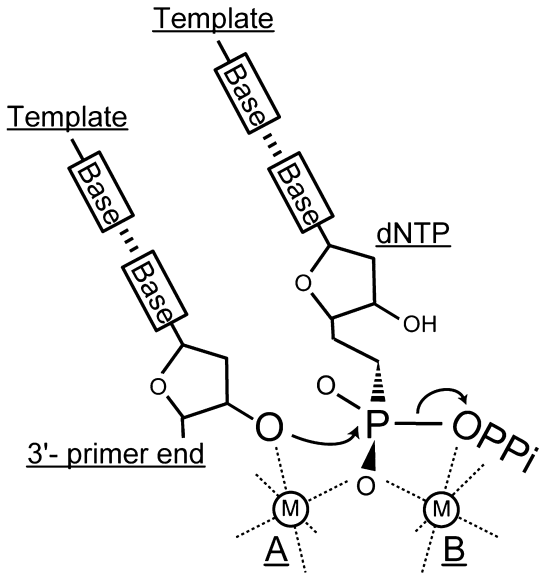


**Figure 3** Two-metal-ion mechanism for the nucleotidyl-transfer reaction. "A" and "B" indicate the A- and B-metal binding site, respectively.

complementary dNTP to the templating base is incorporated and the phosphate group of dNTP binds to the structurally conserved two carboxylates in the palm domain through two divalent cations ($Mg^{2+}$ or $Ca^{2+}$), and the primer 3′ terminus, dNTP and two divalent cations are aligned for the reaction (Fig. 1). The structural and biochemical insights have greatly contributed to the understanding of a mechanism for the nucleotidyl-transfer reaction (Fig. 3). Based on the mechanism, the 3′-OH at the primer end attacks the α phosphorus of an incoming dNTP. After that, a new phosphodiester bond is formed between the 3′-OH and the α phosphorus, and the phosphodiester bond between the α- and β-phosphates of dNTP is broken. This reaction has been shown to require two $Mg^{2+}$ ions (The binding sites are called A- and B-site, respectively, Fig. 3) and is the $S_N2$-type involving a pentacovalent phosphate intermediate. In the case of the other divalent cations, $Mn^{2+}$, which adapts octahedral geometry similar to $Mg^{2+}$, also activates the reaction, and $Ca^{2+}$ inhibits the reaction because it prefers to have more than six ligands with longer coordination distances.

The two-metal ion mechanism was proposed on the basis of the pre-reaction structures of polymerase-substrate complexes using substrate analogs (dideoxynucleotide at the primer end or non-hydrolysable dNTP) or a divalent cation such as $Ca^{2+}$, and these analogs sometimes distort the active site geometry for the reaction. Although there are reports that addition of dNTPs in the crystals of DNA polymerase I induces primer extension *in crystallo*[12,13], the actual process of the nucleotidyl-transfer reaction has never been visualized.

## Structural feature of human DNA polymerase η

Human DNA polymerase η (Pol η), encoded by the Xeroderma pigmentosum variant (XPV) gene (also known as POLH), is a member of the Y-family DNA polymerases and is involved in translesion synthesis through cyclobutane pyrimidine dimers (CPDs) generated by ultraviolet light[14]. Recent structural studies of Pol η revealed the structural basis for the detailed consecutive steps during the translesion synthesis through CPDs as well as cisplatin adduct[15,16]. Overall structure of Pol η (catalytic domain, 1–432 amino acids) in complex with normal DNA and dAMPNPP (a non-hydrolysable dATP analog) is shown in Figure 2a. Like the other Y-family DNA polymerases, Pol η consists of the palm, finger, thumb and little finger domains. The thumb and little finger domains interact with a double-stranded DNA. The thumb domain contacts the backbone of the primer strand, and the little finger domain interacts with the major groove of DNA. The finger domain contacts the replicating base pair and an incoming dAMPNPP. Similar to the other Y-family DNA polymerases, the finger and thumb domains of Pol η are smaller than those of replicative DNA polymerases, that leads to a relatively open and solvent exposed active site in the palm domain. In the active site, two $Mg^{2+}$ with ideal octahedral geometry are coordinated to

the 3′-OH of the primer terminus, three conserved carboxylates (Asp13, Asp115 and Glu116) and the phosphate group of dAMPNPP (Fig. 2b). The 3′-OH, which is 3.2 Å from the α-phosphorus of dAMPNPP, poises for in-line nucleophilic attack.

## Visualization of the nucleotidyl-transfer reaction by Pol η

Time-resolved protein crystallography is a powerful method to directly observe structural changes during enzymatic reaction and understand how enzymes function at atomic resolution[17]. In order to observe enzymatic reaction by time-resolved protein crystallography, it is very important to find out crystallization and reaction conditions which are satisfied with the following points: 1) Obtain crystals of an enzyme-substrate complex in which a substrate in the active site is pre-aligned for reaction. 2) Control reaction rate to follow whole reaction process in observable time scale because enzymatic reaction is in general very fast. In addition, conformational changes during reaction often cause crystal decay, and enzymes with limited conformational change are preferred. Therefore, in order to follow the nucleotidyl-transfer reaction of DNA polymerase *in crystallo*, we focused on the characteristic features of Pol η, which are the slow reaction rate and limited conformational change during the reaction. The catalytic rate of Pol η is at least 100-fold lower than those of replicative DNA polymerases[18,19]. Also, in contrast to the A-, B-, X-family DNA polymerases whose finger domain undergoes a conformational change from an open to a closed state by binding of dNTP, Pol η does not show any appreciable conformational change induced by the dNTP binding[20,21]. In addition, the Pol η crystal has diffraction quality (~1.5 Å resolution) high enough to discuss detailed structural changes. Taking advantage of these features of Pol η, we visualized the nucleotidyl-transfer reaction by time-resolved protein crystallography using the Pol η crystal.

First, we examined the pH dependency of the catalytic rate of Pol η in solution. Pol η exhibits a bell-shaped pH-dependence curve, and the catalytic rate of Pol η is quite low at pH 6.0 and rises with increasing pH. Therefore, we crystallized the Pol η–substrate complex (Pol η–DNA–dATP) at pH 6.0 and in the presence of inhibitory $Ca^{2+}$ in order to prevent the nucleotidyl-transfer reaction. The structure of Pol η–DNA–dATP– $Ca^{2+}$ equilibrated at pH 6.8 was determined at 1.50 Å. As expected, there is no nucleotidyl-transfer reaction. In the active site, a $Ca^{2+}$ ion clearly occupies at the B site while the A site has very low occupancy of a metal ion (Fig. 4a). In the absence of the A site metal ion, Glu116 has alternative conformations and the 3′-OH at the primer end is 4.2 Å away from the α phosphorus of dATP. Arg61, which has multiple conformations in the dAMPNPP complex[15,16], binds tightly to dATP with two hydrogen bonds. The structure is termed the ground-state.

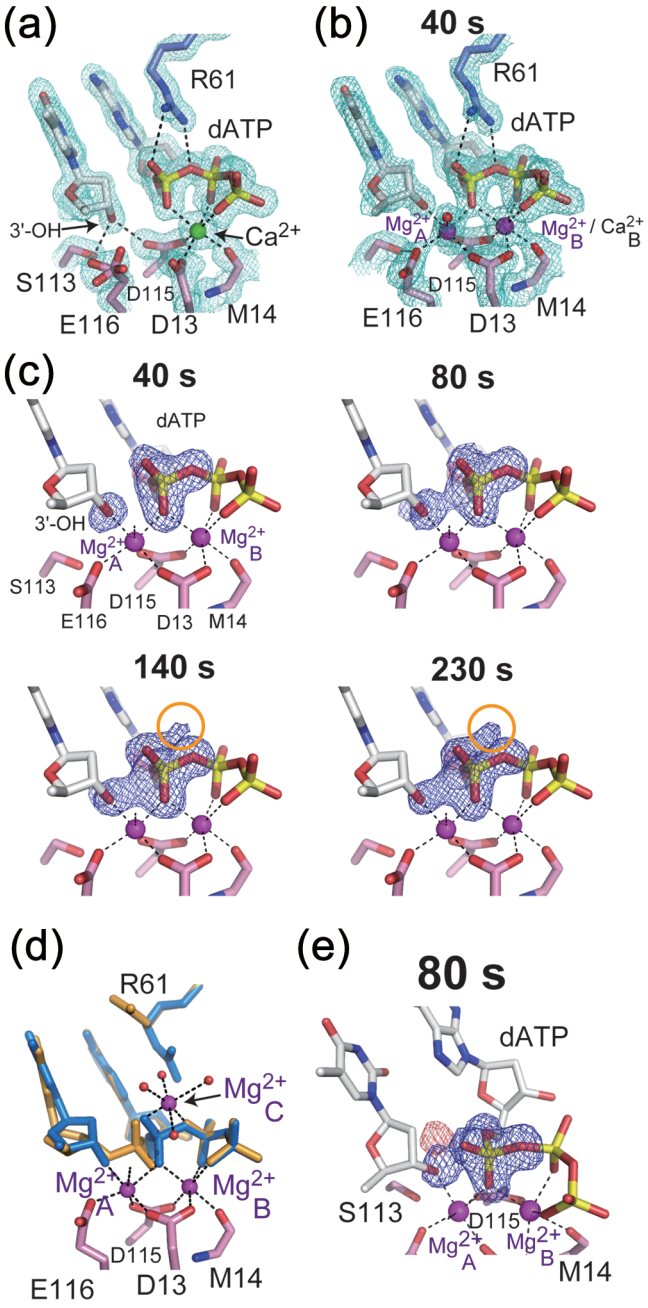


**Figure 4** Structures and electron densities during the reaction. (a) Active site in the ground-state. The $2F_o–F_c$ map contoured at 1.2 σ is shown as a cyan mesh. $Ca^{2+}$ is shown as a green sphere. (b) Active site in the refined 40-s structure. The $2F_o–F_c$ map contoured at 1.2 σ is shown as a cyan mesh. $Mg^{2+}$ is shown as a purple sphere. (c) Electron density around the new bond at each time point. The $F_{o(40–230\ s)}–F_{c(40\ s)}$ omit maps contoured at 4 σ are overlaid on the 40-s structure. The electron densities corresponding to the third $Mg^{2+}$ are indicated by orange circles. (d) Refined 230-s structure at 1.52 Å resolution. The reactant state and product state are shown in blue and orange, respectively. (e) Position of a transient water molecule. The $F_o–F_c$ omit map at 80 s (4 σ) is shown as a mesh, and the electron density corresponding to a transient water molecule is shown in red.

Based on the bell-shaped pH-dependence curve in solution, we examined the catalytic rate *in crystallo* by changing pH (6.5–7.2 in 0.1 or 0.2 increments) and the concentration of $Mg^{2+}$ (0.1, 0.5 and 1.0 mM), and confirmed that the condition at pH 6.8–7.0 with 1 mM $Mg^{2+}$ is most suitable to observe the nucleotidyl-transfer process in 300 s. The procedure of the nucleotidyl-transfer reaction *in crystallo* is as follows. 1) Pre-incubate crystals at pH 6.8 or 7.0 in order to change pH for the reaction. 2) Initiate the reaction by transferring crystals to a pH 6.8 or 7.0 reaction buffer containing 1 mM $Mg^{2+}$. 3) Terminate the reaction by freezing at 77 K after incubation at 293 K for 40 to 300 s (~40-s intervals). 4) Solve the intermediate structures.

After 40 s, $Mg^{2+}$ binds to the A site and concomitantly the side chains of Glu116 and Asp13 rotate for the $Mg^{2+}$ binding (Fig. 4b). The 3′-OH also coordinates to the A-site $Mg^{2+}$ ion, and is closer to the α phosphorus in 3.2 Å. This active site structure is almost identical to that in the dAMPNPP complex. The 3′-OH, dATP and two $Mg^{2+}$ are aligned for the reaction within 40 s, but a new bond formation has not occurred yet because there is no positive peak between the 3′-OH and the α phosphorus. The electron density corresponding to a new bond begins to appear at 80 s, and increases over time (Fig. 4c). Intermediate structures obtained between 80 to 300 s were refined as a mixture of the reactant state and the product state (immediately before and after the nucleotidyl-transfer) at different ratios. For example, the 230-s structure could be refined with 40% reactant state and 60% product state (Fig. 4d). Comparison of the reactant and product state clearly shows the structural changes during reaction. After the new bond formation, the sugar pucker at the primer end changes from C2′-endo conformation to C3′-endo conformation, and the α-phosphate of dATP moves 1.4 Å toward the primer end. Accompanied with the shift of the α-phosphate, Arg61 flips toward the solvent and is replaced by an arriving new metal ion (discussed later).

In the reaction process, two unexpected electron densities are observed. The first emerges after 140 s and is close to the α-phosphate of dATP at the opposite side of the A- and B-metal binding sites (Fig. 4c, orange circles). The refined 230-s structure at 1.52 Å resolution indicates that this is a $Mg^{2+}$ ion because of its short coordination distances and the octahedral geometry (Fig. 4d). This third $Mg^{2+}$ ($Mg^{2+}_C$) is located at the space of the departed Arg61. $Mg^{2+}_C$ is coordinated to the oxygen of the α-phosphate, the leaving oxygen, and four water molecules, indicating that $Mg^{2+}_C$ neutralizes the negative charge in the reaction intermediates. The second emerging sphere appears after 80 s and is close to the 3′-OH (Fig. 4e, a red mesh). This position is within hydrogen-bonding distance with the 3′-OH, and is interpreted as a water molecule. The density of this water molecule declines drastically after 140 s when the product state becomes prominent. This is because there is a steric hindrance between the water and the C3′-endo conformation in the product state. This water molecule appears immediately before the new bond formation, and seems to be involved in the deprotonation of the 3′-OH. Another candidate for the deprotonation of the 3′-OH is Ser113, which is hydrogen-bonded with the 3′-OH in the ground-state (Fig. 4a). However, our mutational study showed the S113A mutant retains 95% of the $k_{cat}$ value of the wild-type. Therefore we proposed that two $Mg^{2+}$ ions and the alignment of the 3′-OH and the incoming dNTP promote the deprotonation of the 3′-OH, and the proton is transferred to the transient water molecule.

Based on the structural insights obtained from the time-resolved protein crystallography of Pol η, we can sketch a detailed reaction pathway for metal-ion-dependent polymerase reaction (Fig. 5). First, after DNA and dNTP binding to the polymerase, $Mg^{2+}$ binds to the A-site to align the 3′-OH and dATP for the reaction. A water molecule moves in and binds to the 3′-OH, and the deprotonation of the 3′-OH is activated by the metal ions and assisted by the water and dNTP. After the nucleophilic attack by the nucleophile, a new bond is formed between 3′-OH and the α-phosphorus of dNTP during which the conformation of the primer end converts from C2′-endo to C3′-endo. A third $Mg^{2+}$ replaces Arg61 to stabilize the reaction intermediates.

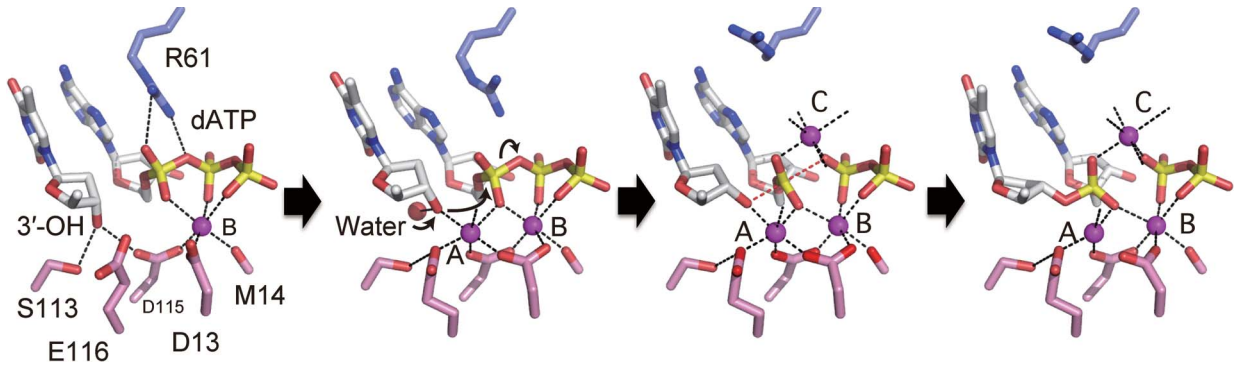


**Figure 5** A new proposed mechanism for the nucleotidyl-transfer reaction.

## Concluding remarks

So far, the mechanism of the nucleotidyl-transfer reaction in DNA polymerase has been suggested on the basis of the crystal structures of the catalytic intermediate mimics with substrate analogs. This time, we have succeeded in visualizing the time course of the reaction in DNA polymerase in real time and at atomic resolution, and new structural features are revealed, including arrival of a water molecule to assist deprotonation of the 3′-OH at the primer end and an additional $Mg^{2+}$ to stabilize the intermediate state. These results show the importance of observing the actual reaction process by time-resolved protein crystallography. However, there remains the question whether the reaction pathway proposed in our study is shared with the other DNA polymerases. Further studies on DNA polymerases using time-resolved protein crystallography and molecular dynamics will answer the question.

## References


1. Foti, J. J. & Walker, G. C. SnapShot: DNA polymerases I prokaryotes. *Cell* **141**, 192–192.e1 (2010).
2. Foti, J. J. & Walker, G. C. SnapShot: DNA polymerases II mammals. *Cell* **141**, 370–370.e1 (2010).
3. Steitz, T. A. & Steitz, J. A. A general two-metal-ion mechanism for catalytic RNA. *Proc. Natl. Acad. Sci. USA* **90**, 6498–6502 (1993).
4. Brautigam, C. A. & Steitz, T. A. Structural and functional insights provided by crystal structures of DNA polymerases and their substrate complexes. *Curr. Opin. Struct. Biol.* **8**, 54–63 (1998).
5. Rothwell, P. J. & Waksman, G. Structure and mechanism of DNA polymerases. *Adv. Protein Chem.* **71**, 401–440 (2005).
6. Yang, W., Lee, J. Y. & Nowotny, M. Making and breaking nucleic acids: two-$Mg^{2+}$-ion catalysis and substrate specificity. *Mol. Cell* **22**, 5–13 (2006).
7. Nakamura, T., Zhao, Y., Yamagata, Y., Hua, Y. J. & Yang, W. Watching DNA polymerase η make a phosphodiester bond. *Nature* **487**, 196–201 (2012).
8. Li, Y., Korolev, S. & Waksman, G. Crystal structures of open and closed forms of binary and ternary complexes of the large fragment of Thermus aquaticus DNA polymerase I: structural basis for nucleotide incorporation. *EMBO J.* **17**, 7514–7525 (1998).
9. Franklin, M. C., Wang, J. & Steitz, T. A. Structure of the replicating complex of a pol alpha family DNA polymerase. *Cell* **105**, 657–667 (2001).
10. Batra, V. K., Beard, W. A., Shock, D. D., Krahn, J. M., Pedersen, L. C. & Wilson, S. H. Magnesium-induced assembly of a complete DNA polymerase catalytic complex. *Structure* **14**, 757–766 (2006).
11. Yang, W. Damage repair DNA polymerases Y. *Curr. Opin. Struct. Biol.* **13**, 23–30 (2003).
12. Kiefer, J. R., Mao, C., Braman, J. C. & Beese, L. S. Visualizing DNA replication in a catalytically active Bacillus DNA polymerase crystal. *Nature* **391**, 304–307 (1998).
13. Johnson, S. J., Taylor, J. S. & Beese, L. S. Processive DNA synthesis observed in a polymerase crystal suggests a mechanism for the prevention of frameshift mutations. *Proc. Natl. Acad. Sci. USA* **100**, 3895–3900 (2003).
14. Masutani, C., Kusumoto, R., Yamada, A., Dohmae, N., Yokoi, M., Yuasa, M., Araki, M., Iwai, S., Takio, K. & Hanaoka, F. The XPV (xeroderma pigmentosum variant) gene encodes human DNA polymerase eta. *Nature* **399**, 700–704 (1999).
15. Biertümpfel, C., Zhao, Y., Kondo, Y., Ramón-Maiques, S., Gregory, M., Lee, J. Y., Masutani, C., Lehmann, A. R., Hanaoka, F. & Yang, W. Structure and mechanism of human DNA polymerase eta. *Nature* **465**, 1044–1048 (2010).
16. Zhao, Y., Biertümpfel, C., Gregory, M. T., Hua, Y. J., Hanaoka, F. & Yang, W. Structural basis of human DNA polymerase η-mediated chemoresistance to cisplatin. *Proc. Natl. Acad. Sci. USA* **109**, 7269–7274 (2012).
17. Petsko, G. A. & Ringe, D. Observation of unstable species in enzyme-catalyzed transformations using protein crystallography. *Curr. Opin. Chem. Biol.* **4**, 89–94 (2000).
18. Patel, S. S., Wong, I. & Johnson, K. A. Pre-steady-state kinetic analysis of processive DNA replication including complete characterization of an exonuclease-deficient mutant. *Biochemistry* **30**, 511–525 (1991).
19. Wong, I., Patel, S. S. & Johnson, K. A. An induced-fit kinetic mechanism for DNA replication fidelity: direct measurement by single-turnover kinetics. *Biochemistry* **30**, 526–537 (1991).
20. Yang, W. & Woodgate, R. What a difference a decade makes: insights into translesion DNA synthesis. *Proc. Natl. Acad. Sci. USA* **104**, 15591–15598 (2007).
21. Ummat, A., Silverstein, T. D., Jain, R., Buku, A., Johnson, R. E., Prakash, L., Prakash, S. & Aggarwal, A. K. Human DNA polymerase η is pre-aligned for dNTP binding and catalysis. *J. Mol. Biol.* **415**, 627–634 (2012).